Air-Diffusion-Channel Constrained Surface Based Stereolithography for Three-Dimensional Printing of Objects With Wide Solid Cross Sections

Haiyang He
Department of Mechanical and Industrial Engineering,
The University of Illinois at Chicago,
Chicago, IL 60607

Yayue Pan[1]
Department of Mechanical and Industrial Engineering,
The University of Illinois at Chicago,
2039 Engineering Research Facility,
842 W. Taylor Street,
Chicago, IL 60607
e-mail: yayuepan@uic.edu

Alan Feinerman
Department of Electrical and Computer Engineering,
The University of Illinois at Chicago,
Chicago, IL 60607

Jie Xu
Department of Mechanical and Industrial Engineering,
The University of Illinois at Chicago,
Chicago, IL 60607

Oxygen inhibition has been proved capable of reducing the separation force and enabling successful prints in constrained surface vat photopolymerization (CSVP) based three-dimensional (3D) printing processes. It has also been demonstrated as a key factor that determines the feasibility of the newly developed CSVP-based continuous 3D printing systems, such as the continuous liquid interface production. Despite its well-known importance, it is still largely unknown regarding how to control and enhance the oxygen inhibition in CSVP. To close this knowledge gap, this paper investigates the constrained surface design, which allows for continuous and sufficient air permeation to enhance the oxygen inhibition in CSVP systems. In this paper, a novel constrained surface with air-diffusion-channel is proposed. The influences of the air-diffusion-channel design parameters on the robustness of the constrained surface, the light transmission rate, and light intensity uniformity are studied. The thickness of the oxygen inhibition layer associated with the proposed constrained surface is studied analytically and experimentally. Experimental results show that the proposed air-diffusion-channel design is effective in maintaining and enhancing the oxygen-inhibition effect, and thus can increase the solid cross section size of printable parts. [DOI: 10.1115/1.4039440]

Keywords: air-diffusion-channel, constrained surface, vat photopolymerization, stereolithography (SL), oxygen inhibition, wide solid cross section

1 Introduction

Additive manufacturing, also known as three-dimensional (3D) printing or direct digital manufacturing, is a class of technologies that fabricate a three-dimensional physical model directly from its digital design, by accumulating materials, usually in a layer-by-layer way. A number of additive manufacturing techniques have been developed for processing metal [1–4], polymer [5–7], ceramic [8], bio- materials [9], and even multiple materials [10,11], for a wide range of applications. Recently, constrained surface-based stereolithography (SL), is gaining wide attention and has been widely applied in many fields, including medical device, aerospace, education, and consumer product fields [5–8]. In constrained surface SL, a thin layer of liquid photopolymer is constrained between the platform or part and the constrained window. The ultraviolet (UV) light penetrates the transparent constrained surface and cures the liquid polymer. Currently, the two most widely used classes of constrained surfaces are: (1) glass or acrylic plate coated with polydimethylsiloxane (PDMS) [8,12–18] and (2) air permeable film that is clamped and tensioned, due to the relatively low cost, ease of fabrication, good oxygen permeability, and excellent optical transparency. The oxygen permeability of constrained surface is critical to the reliability and robustness of the system, and the printable geometries [19]. Research studies have demonstrated that the oxygen inhibition effect is beneficial to both conventional layer-by-layer SL and newly reported continuous SL processes. For conventional layer-by-layer SL process, the separation of a newly cured layer from the constrained surface is a well-known technical barrier that greatly limits the printable size, process reliability, and print speed. In Ref. [20], it is found that the oxygen permeability of PDMS is strongly correlated to the separation mechanism in the manufacturing process. Higher oxygen level in the vicinity of the PDMS surface would facilitate the separation process and thus avoid damage to the printed layers or damage to the constrained surface. In Ref. [21], the oxygen permeability of the tensioned film plays a significant role in determining the feasibility of layerless SL process. The principle for this oxygen inhibition phenomenon has been elaborated by the work in Ref. [22]. It is found that the oxygen can inhibit free radical photopolymerization reactions by reacting with radical species in photopolymers, which form the oxygen inhibited layer. This reaction results in an uncross-linked "lubrication layer" close to the constrained surface, which assists the separation of newly cured layer from the constrained surface in conventional SL and also enables the continuous SL. Thus, controlling the oxygen level above the constrained surface is critical.

Various methods have been implemented to modify the oxygen level above the constrained surface in SL systems, such as using highly air permeable teflon film [21], or adding an external oxygen supplying system to the PDMS film [23]. The effect of PDMS composition on its permeation properties to air has also been investigated [24]. It is found that, by increasing the base polymer mixing ratio, the air permeability can be increased by up to 300% of the permeability of the PDMS surface made by the standard 10 base polymer: one curing agent weight ratio composition. Surface modification methods for modifying the oxygen permeability of PDMS films have been reviewed in Ref. [25]. However, with all those methods, oxygen supply offered by PDMS-based constrained surface is still limited. Although it has shown that constrained surfaces based on the highly permeable Teflon AF 2400 can supply sufficient oxygen and hence a thick oxygen inhibition layer, this kind of constrained surfaces has other problems such as

[1]Corresponding author.

Manuscript received June 21, 2017; final manuscript received February 14, 2018; published online April 2, 2018. Assoc. Editor: Sam Anand.

tensioning challenge, and creases of the film. To summarize, despite recent advances on materials and hardware design, it is an important challenge to achieve controllable oxygen level in constrained surface vat photopolymerization (CSVP), limiting the manufacturing process stability, robustness, and printing volume of the related 3D printing technologies.

This paper investigates a novel PDMS-based constrained surface design, in which air-diffusion-channel is introduced for continuous oxygen supply. Section 2 presents the design in detail. Effects of design parameters on constrained surface strength, light transmission rate, and uniformity are studied in Secs. 3 and 4. In Sec. 5, effects of the air-diffusion-channel design parameters on the oxygen inhibition layer thickness are modeled and experimentally measured. Section 6 performs experiments and validates the effectiveness of the proposed constrained surface for fabricating objects with wide solid cross sections in vat photopolymerization apparatus, through comparing the fabrication results with conventional constrained surface.

2 A Novel Polydimethylsiloxane Constrained Window With Air-Diffusion-Channel Design

In our previous study on constrained surface SL process, we found that as the printing process proceeds, the oxygen inhibition layer gets thinner due to the oxygen consumption in printing, leading to increasing separation force and hence failures in the printing process. It is also found that a porous substrate with PDMS coating is possible to address this challenge by providing direct contact of the air and PDMS and thus supplying the oxygen continuously. Preliminary study has proved the feasibility of using the porous transparent substrate coated with PDMS film as the constrained surface in SL [20]. Hence, this paper will further investigate how to design such porous PDMS-coated constrained surfaces, and how the various design parameters will affect the performance of the constrained surface in SL process.

To enhance the oxygen permeability and the mechanical strength of the constrained window, microscale holes are made through the transparent substrate, serving as microscale air channels, and then with a layer of PDMS is coated on the porous transparent substrate. As illustrated in Fig. 1, three types of air-diffusion-channel structures can be fabricated, with design parameters including the top opening diameter D_T and the bottom opening diameter D_B of the air channels, the depth h of the air channels, the period along X direction W_x, and along Y direction W_y. In the first air-channel structure design, the air channels are straight through holes, with equal D_{1T} and D_{1B}. Structure 2 is an inverted cone design, with D_{2T} larger than D_{2B}, while structure 3 is a circular truncated cone design, in which D_{3T} is smaller than D_{3B}. In our study, laser machining is used to fabricate the air channels. In order to understand the effects of through-hole geometry, this investigation focuses on the latter two designs.

Optically clear acrylic plates with air-diffusion-channel were prepared using a 100 W X2-600 CO_2 laser machine from Universal Laser Systems (Scottsdale, AZ). Figure 2(*a*) shows the microscopic side views of some prepared air-diffusion-channel samples.

A 48 W CO_2 laser with a scanning speed of 8.7 mm/s was used to machine the micropores in a 4.5 mm thick acrylic sheet. The laser machining process generated holes with larger openings on the top and smaller openings on the bottom, due to the nonuniform energy distribution along the laser beam direction. With a spot size of 0.13 mm, by adjusting the scanning speed, the laser can fabricate holes through the acrylic plate, with top opening diameters ranging from 0.2 mm to 1.4 mm and bottom opening diameters ranging from 0.07 mm to 1.3 mm. To prepare a constrained window with the air-diffusion-channel structure 2, a layer of PDMS film was coated on the machined acrylic plate surface with a larger through hole openings. To prepare a constrained window with the air-diffusion-channel structure 3, the machined acrylic plate was turned over and a layer of PDMS film was coated on the side with smaller through hole openings.

The PDMS coating was made by mixing the base polymer with curing agent with a 10:1 weight ratio. The PDMS-coated acrylic plate was then used as the bottom surface of the liquid resin vat and a constrained surface in the CSVP processes. Figure 2(*b*) shows the top view of a microscale-air-channel acrylic plate sample coated with PDMS. A prepared resin vat with such an air-diffusion-channel-based constrained window is shown in Fig. 2(*c*). The air-diffusion-channel on the acrylic substrate, combined with the good oxygen permeability of PDMS expedited the diffusion of oxygen to the liquid resin and enhanced the oxygen inhibition effect during the printing process.

As introduced in Sec. 1, the constrained surface in vat photopolymerization-based 3D printing systems needs to meet three requirements: (1) optically clear, so that the light can penetrate it and cure the liquid resin, (2) oxygen permeable, so that an oxygen inhibition layer can be formed and the newly cured resin could separate from the constrained surface and stick to the previously cured resin, and (3) mechanically strong, so that it could withstand various forces, especially the force-induced during the procedure that the newly cured layer is separated from it. Common failures of current constrained windows include: (1) tensioning failure or creases for constrained windows made by tensioned Teflon films; (2) broken coating or separation of coating from the substrate, for constrained windows made by PDMS-coated plates; (3) insufficient or unstable oxygen permeation. To investigate how the proposed novel constrained window design can address the above challenges, Secs. 3–5 analyze the effects of various design parameters on the mechanical strength, the light transmission and uniformity, and the oxygen permeation rate of the constrained surface. Both theoretical analysis and experimental study have been performed.

3 Effect of Air-Diffusion-Channel Design Parameters on Mechanical Strength

To avoid the common failures of broken or separated PDMS coating, the mechanical strength, especially the bonding strength, between the PDMS coating and the substrate with air-diffusion-channel needs to be assessed. Influences of air-diffusion-channel design parameters on the bonding strength are analyzed and tested in this section.

Compared with the conventional PDMS constrained surface, the proposed three designs of air-diffusion-channel structures, illustrated by structures 1, 2, and 3 in Fig. 1, make better use of

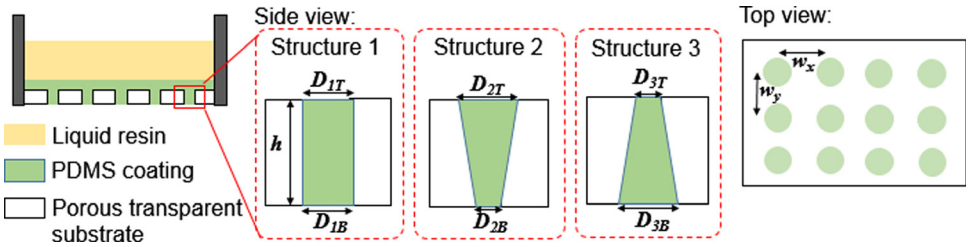

Fig. 1 Schematic drawing of the air-diffusion-channel design in PDMS-based constrained window

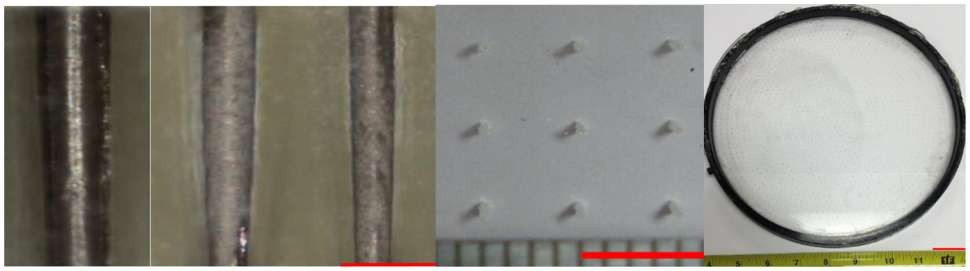

(*a*) (*b*) (*c*)

Fig. 2 (*a*) Microscopic images of the side view of the prepared air-diffusion-channel samples. Scale bar: 1 mm; (*b*) top view of a air-diffusion-channel sample coated with PDMS. Scale bar: 5 mm; (*c*) a prepared liquid vat with air-diffusion-channel-based constrained surface on the bottom. Scale bar: 1 in.

the Van der Waals force and increase the contact area between PDMS coating and the acrylic substrate surface [26–28]. Besides, the cone channel design (structure 3) further increases the mechanical adhesion between the PDMS and the substrate. Accordingly, the bonding force between the PDMS coating and the acrylic plate substrate with the air-diffusion-channel designs can be expressed as following:

$$F_{\text{bonding}} = F_{\text{Vander Waals}} + F_{\text{Mechanical Lock}} \tag{1}$$

where the $F_{\text{Van der Waals}}$ is assumed to be proportional to the contact area between the PDMS and acrylic substrate, and $F_{\text{Mechanical Lock}}$ only exists for the design structure 3. Thus, the bonding force for designs 2 and 3 can be expressed in the following equations, respectively

$$F_{\text{bonding2}} = N * (p * \text{l} * (R + r) - p * r^2) * c \tag{2}$$

$$F_{\text{bonding3}} = N * (p * \text{l} * (R + r) - p * R^2) * c + F_{\text{Mechanical Lock}} \tag{3}$$

where R and r are the radiuses of the openings at the two ends of the air-diffusion-channels. As illustrated in Fig. 1, $D_{2T} = D_{3B} = 2R$, $D_{2B} = D_{3T} = 2r$), N is the number of air channels, and c is a constant. Thus,

$$F_{\text{bonding3}} - F_{\text{bonding2}} = N * c * p * (R^2 - r^2) + F_{\text{Mechanical Lock}} \tag{4}$$

From Eq. (4), it can be seen that the bonding force for design 3 is larger than that of design 2. To verify it, acrylic substrates with air-diffusion-channel structure 2 and acrylic substrates with air-diffusion-channel structure 3 are prepared. The acrylic substrate is a 40 mm diameter round plate with a thickness of 4.5 mm. The diameter of the prepared air-diffusion-channel is $D_{2T} = D_{3B} = 0.8$ mm. A PDMS film with a thickness of 2 mm is coated on the acrylic substrate, and a PDMS cube is made on the coating center for the top gripping in the mechanical strength test. The acrylic substrate bottom surface is bonded to an acrylic handle for the bottom gripping in the mechanical strength test. The mechanical test setup is shown in Fig. 3.

Constrained windows with different air-diffusion-channel designs and PDMS coating were prepared and tested using universal testing machine from INSTRON (Norwood, MA). The maximum pulling force that was applied before separating the PDMS coating from the acrylic substrate was measured. As shown in Fig. 4, the measured maximum pulling force before breaking the bonding between PDMS and acrylic substrate are 19.82 N, 35.61 N, and 64.07 N, for the PDMS-coated constrained window with no air channel in the acrylic substrate, and with air channel designs 2 and 3 in acrylic substrates, respectively. The experimental results reveal that the air-diffusion-channel structure design 3 is superior in terms of the bonding strength. It can address the PDMS coating separation issue much more effectively than the existing PDMS-coated constrained surface design and the proposed constrained surface design with air-diffusion-channel structure design 2.

4 Effect of Air-Diffusion-Channel on Light Transmission and Uniformity

Light transmission of the constrained surface is crucial to vat photopolymerization process [29]. To investigate the effects of

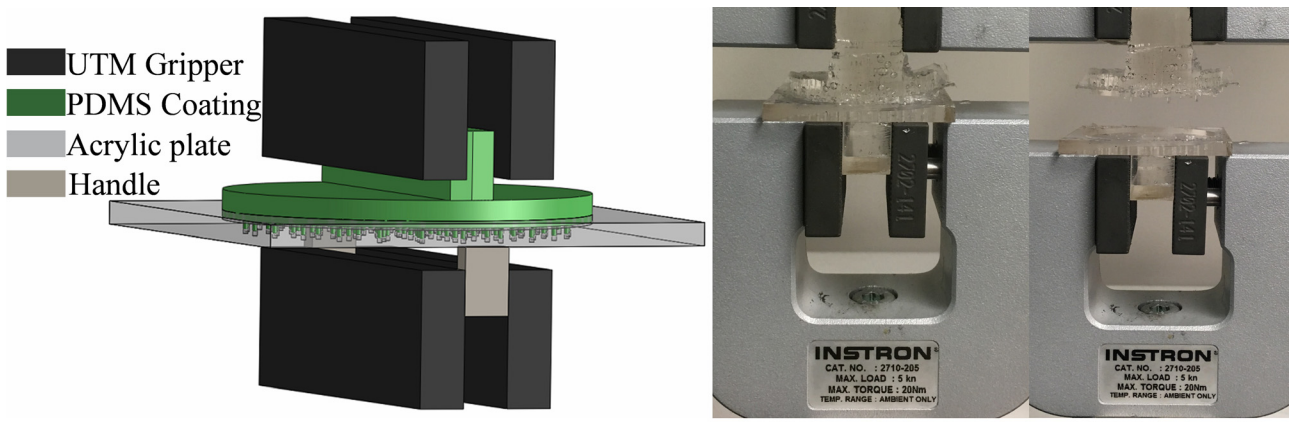

(*a*) (*b*) (*c*)

Fig. 3 (*a*) Illustration of the bonding force test setup, (*b*) experimental setup for bonding force testing before the test, and (*c*) photo of the bonding force testing setup when the PDMS coating was separated from the bottom substrate

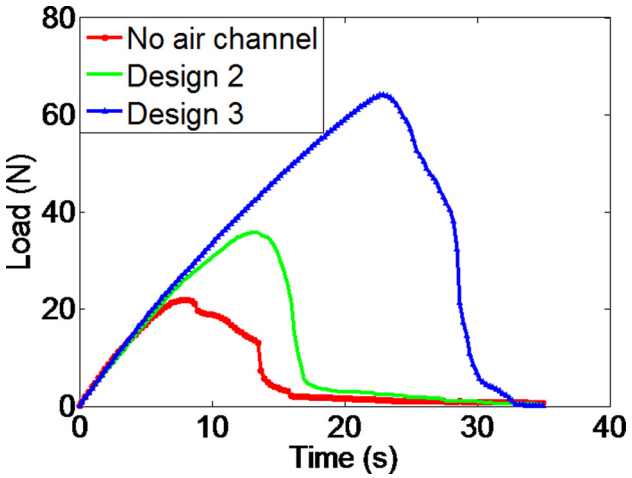

Fig. 4 Bonding force measurement for three different constrained surface designs

the air-diffusion-channel on the light transmission performance of the constrained surface, the transmitted optical power is measured for the air-diffusion-channel based constrained window designs. Constrained surface samples with varied air-diffusion-channel designs were manufactured using the laser micromachining process presented in Sec. 2. Air-diffusion-channel with diameters of 0.4 mm, 0.5 mm, and 0.74 mm for both D_{2T} and D_{3B} were prepared on 4.5 mm thick acrylic substrates. Then, 2 mm thick PDMS films were coated on these laser machined substrates. To make comparisons [30,31], conventional constrained surfaces were also prepared by coating 2 mm thick PDMS layers on 4.5 mm acrylic substrates which had no microscale through-holes.

An optical power and energy meter, PM200 from Thorlabs, was used to measure the light energy passing through the prepared constrained surfaces with air-diffusion-channels and the conventional constrained surfaces without air-diffusion-channels. The measured light wavelength was set to be 405 nm [32–34]. A diaphragm was placed in the light path of the light projection unit. The size of the diaphragm's aperture regulated the amount of light that passed through a certain area of the constrained window. The aperture's diameter was adjusted to be ~3 mm and the center of the diaphragm's aperture coincided with the axis of the air-diffusion-channel.

The measured optical power data were plotted in Fig. 5. The first three subplots show the comparison between air-diffusion-channel designs 2 and 3 with varied diameters: $D_{2T} = D_{3B} = 0.4$ mm, 0.5 mm, and 0.74 mm, and $D_{2B} = D_{3T} = 0.38$ mm, 0.43 mm, and 0.64 mm, respectively. It can be seen that the measured power curves for these two designs are close to each other. In the fourth subplot, the measured optical power for constrained surface without air-diffusion-channel is the highest. The average optical power of design 2 and 3 decreases as the diameter of air-diffusion-channel increases from 0.4 mm to 0.74 mm. It is shown that smaller size of air-diffusion-channel tends to have higher transmission rate. The light transmission performance are close for structure designs 2 and 3, though design 3 slightly outperforms design 2 when D_{3B} is smaller than 0.5 mm.

To make a clearer comparison, the light passing through the conventional PDMS constrained window is assumed to have the full light power. The light transmission rate of our proposed constrained surfaces with micro-air channels were calculated by taking the ratio of the average of 100 sampling powers to the full light power. The results are shown in Table 1. It can be seen that the light transmission rates for both designs differ very slightly (within 0.33%) and are sufficiently high (over 98%) for vat photopolymerization.

Light uniformity of the designed constrained surface is also significant to vat photopolymerization process. To investigate the effects of the air-diffusion-channel on the light uniformity, six locations were randomly selected on the six designed constrained surface with air-diffusion-channel, and the light intensities on these six locations were measured. The uniformity ratio E_{max}/E_{min} [35], and the performance of illumination uniformity E_{min} /E_{ave} were then calculated [36]. E_{max}, E_{min}, and E_{ave} denote the maximum, minimum, and average illuminance. The average uniformity ratio and illumination uniformity of six different locations for different air-diffusion-channel were plotted in Fig. 6. The *X*-axis represents different constrained surface designs, from 0.4 mm design 3 (denoted as 0.4 *D*3 in the *X*-axis in Fig. 6) to 0.75 mm design 2 (denoted as 0.75 *D*2 in the *X*-axis in Fig. 6). As shown in Fig. 6, the variation of the uniformity ratio of these six designs is within 0.08%, and the variation of the illumination is within 0.04%. It verified that the proposed air-diffusion-channel design has little influence on the light uniformity.

5 Effect of Air-Diffusion-Channel on Oxygen Inhibition

Oxygen inhibition has been proved useful in vat photopolymerization based 3D printing process. It is of great significance to maintain abundant oxygen adjacent to the constrained surface. Based on the previous research [37], the permeability for a given gas in a given membrane is

$$P = v\delta/(At(p_1 - p_0)) \tag{5}$$

where P is the permeability for a given gas in a given membrane, v is the volume of gas which penetrates through the membrane, δ is the thickness of membrane, A is the area of membrane, t is time, p_1 is the partial pressure of the gas on the higher pressure side of the membrane, and p_0 is the partial pressure of the gas on the lower pressure side of the membrane. Therefore, with the conventional constrained surface, the volume of oxygen penetrated the PDMS film can be obtained by

$$v = PAt\Delta p/\delta \tag{6}$$

With the constrained surface developed in this paper, the volume of the penetrated oxygen v' can be calculated by adding up the volumes of oxygen permeated through the nonporous region and the air-diffusion-channel region

$$v' = v_1 + v_2 = (P_nA_n + P_mA_m)t\Delta p/\delta \tag{7}$$

where P_n is the permeability of the nonporous region which is composed of acrylic substrate and PDMS film; A_n is the area of the nonporous region which is composed of acrylic substrate and PDMS film; P_m and A_m are the permeability and area of the air-diffusion-channel region which is composed of PDMS film only; the sum of A_n and A_m is the area of the constrained surface A; $v_1 = P_nA_nt\Delta p/\delta$represents the volume of oxygen penetrating through nonporous region, and $v_2 = P_mA_mt\Delta p/\delta$represents the volume of oxygen penetrating through the air-diffusion-channel region. Note that the permeability of polymer to oxygen P_n at 25 °C is about 0.5 $\times 10^8 \text{cm}^2/(\text{satm})$, while for PDMS, the permeability P_m is about three orders of magnitude higher than that of the acrylic [38–40].[2] Hence, it can be derived that

$$v' = (P_nA_n + P_mA_m)t\Delta p/\delta \approx P_n(A_n + 10^3 \times A_m)t\Delta p/\delta \gg v = P_nAt\Delta p/\delta \tag{8}$$

The oxygen permeation volume of the newly developed constrained surface is much higher than that of the conventional constrained surface. By rewriting Eq. (8) with the surface area ratio

[2] http://www.goodfellowusa.com/A/Polymethylmethacrylate.html

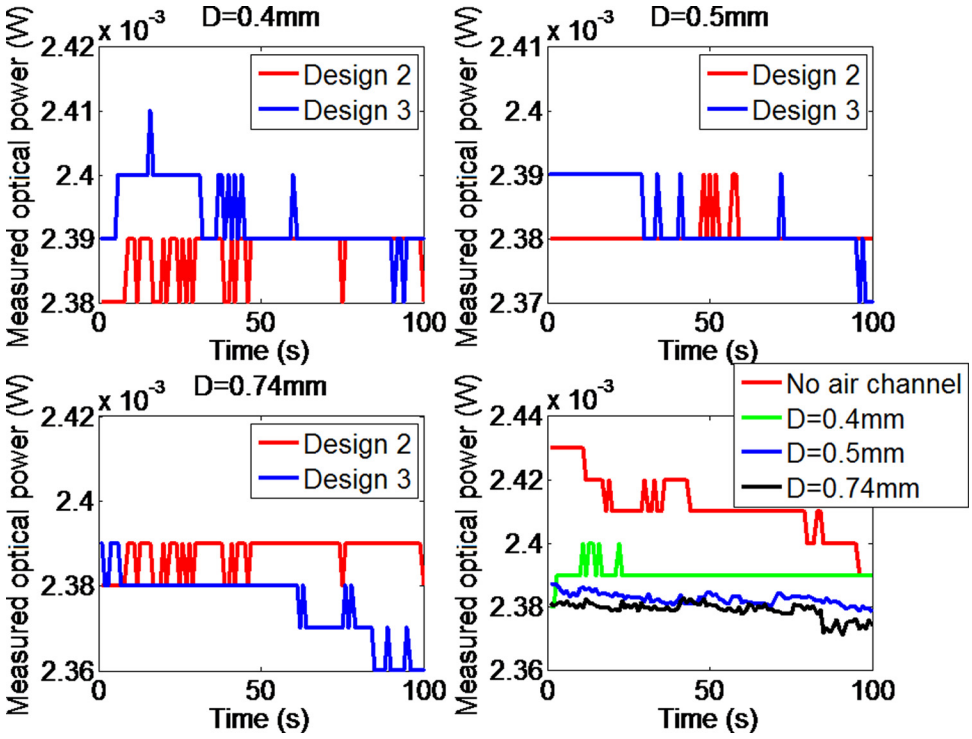

Fig. 5 Optical power measurement results

Table 1 Light transmission rate measurement results

	$D = 0.4$ mm (%)	$D = 0.5$ mm (%)	$D = 0.74$ mm (%)
Design 2	98.98	98.77	98.82
Design 3	99.23	98.84	98.49

of the air-diffusion-channel r and the oxygen layer thickness h', we can get

$$h' = v'/A = [P_n(1-r) + P_m r]t\Delta p/\delta \approx P_m r t\Delta p/\delta = P_m \pi D^2 t\Delta p/(4\delta A) \quad (9)$$

It indicates that the oxygen inhibition layer thickness is approximately linear with the surface area ratio of the air-diffusion-channel r, or the square of the air-diffusion-channel bottom opening diameter D. To validate this relationship between the oxygen inhibition layer thickness and the air-diffusion-channel design, experiments have been performed.

A differential thickness technique was used to measure the oxygen inhibition layer thickness. As illustrated in Fig. 7, in the measurement setup, the liquid photopolymer is sandwiched between the PDMS constrained surface and an impermeable glass with two 500 μm thick brass shims supporting them. To make a comparison between the oxygen inhibition layer thickness of PDMS with and without air-diffusion-channel, different constrained surface samples were prepared and measured. The UV light projecting unit of the SL setup projects a light beam and focuses the light beam on the liquid resin surface near to the PDMS film. The projection time was set at 15 s. Arrays of cylinders of 5 mm diameters were cured. A digital micrometer from Sarrett was used to measure the cured cylinder thickness. The accuracy of the micrometer is 2 μm.

The oxygen inhibition layer thicknesses for micro-air channel designs with bottom opening diameters varied from 0 to 0.8 were measured and plotted in Fig. 8. With a 0 mm air channel diameter, the constrained surface is a conventional design, which has no micro-air channels. The circle in the center of each error bar represents the average value of the measured inhibition layer thickness, which is 18.5 μm, 26.7 μm, 46 μm, 61.5 μm, and 90.0 μm for micro-air channels with diameter $D_{3B} = 0$ mm, 0.2 mm, 0.4 mm, 0.5 mm, and 0.74 mm, respectively. The blue dots are measured results for varied air-diffusion-channel diameters. The red dashed curve is an approximation line by using the fitted

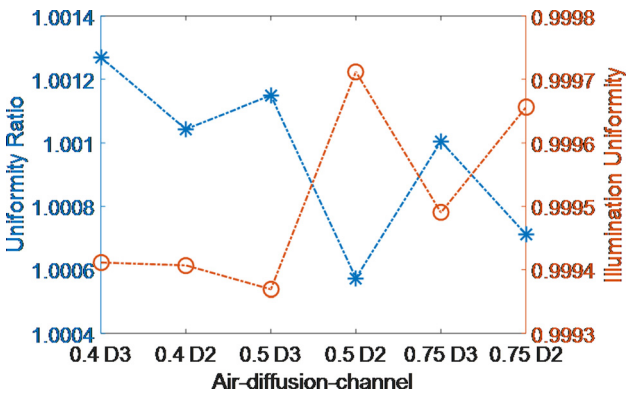

Fig. 6 Light uniformity for different air-diffution-channel designs

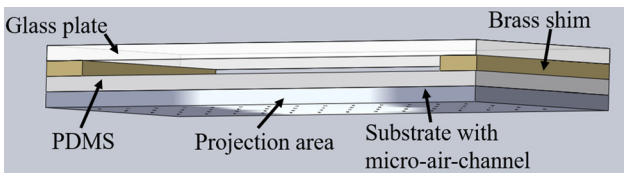

Fig. 7 Schematic of oxygen inhibition layer thickness measurement procedure

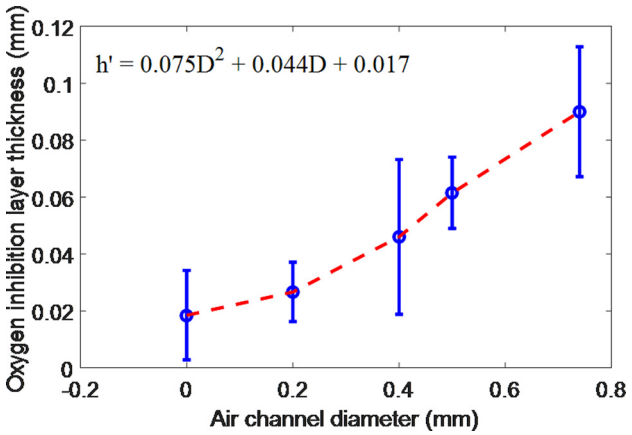

Fig. 8 Results for oxygen inhibition layer thickness measurement

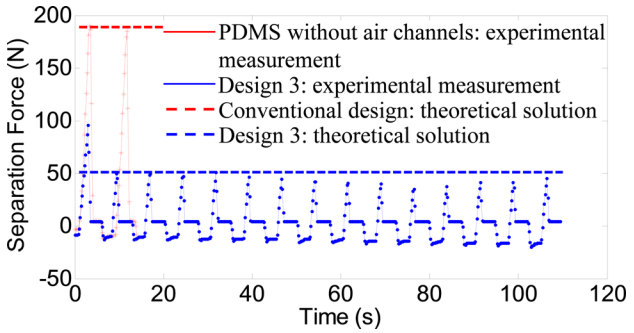

Fig. 10 Separation force for manufacturing a 90 mm diameter using two constrained surfaces

equation of $h' = 0.075D^2 + 0.033D + 0.017$, where h' is the oxygen inhibition layer thickness, and D is the bottom opening diameter of the micro-air channels. It can be seen that the oxygen inhibition layer thickness increases approximately linearly with D^2, the square of the air-diffusion-channel diameter, agreeing well with the theoretical analysis.

6 Experiments and Discussions

6.1 A Bottom–Up Projection Stereolithography Testbed for Constrained Surface Vat Photopolymerization. In Sec. 4, it was found that the structure 2 and structure 3 designs give very similar light transmission performance. However, according to the results in Sec. 5, structure 3 has a better adhesion between the PDMS coating and the porous acrylic substrate and thus providing a mechanically stronger constrained surface. In addition, with a larger air channel diameter, the light transmission rate is decreasing slightly, and the oxygen inhibition layer thickness increases approximately linearly.

For structure 3 design, with a 0.24 mm air channel diameter, the study performed in Sec. 5 found that a ~30 μm thick oxygen inhibition layer could be formed during the printing process. Therefore, in this study, we constructed a bottom–up projection SL testbed, with a newly constrained surface, which has PDMS coated on an acrylic substrate with a structure 3 design air-diffusion-channel, which has $D_{3B} = 0.24$ mm, $D_{3T} = 0.16$ mm. Layer-by-layer 3D printing for production of a solid structure has been performed, with the newly developed air-diffusion-channel-based constrained surface and the conventional constrained surface in the same setup. A schematic of the bottom-up projection SL testbed and the prototype hardware setup are shown in Fig. 9.

6.2 Layer-by-Layer Printing of Objects With Wide Solid Cross Sections. A 90 mm diameter cylinder model was tested to validate the effectiveness of the newly developed air-diffusion-channel-based constrained surface in the bottom–up projection SL system. The model was printed with the newly developed air-diffusion-channel constrained surface and the conventional constrained surface in the same setup. The separation forces during both printing processes were recorded and plotted in Fig. 10.

The red dotted curve is the recorded separation force during the printing process using the conventional constrained surface, which is a PDMS film without air channels. The blue dotted curve is the recorded separation force during the printing process using the newly developed constrained surface, which is a PDMS film with design 3 air-diffusion-channel. The separation force model developed in our previous work [20] has also been used to calculate the theoretical peak separation forces using the two constrained surfaces. The red and blue dashed lines represent the calculated theoretical peak separation forces.

As shown in Fig. 10, the first peak of both separation force curves happened at the moment of separating the first layer, which was cured by a longer exposure time than the curing time of following layers and hence had a relatively larger separation force. It can be seen that the red separation force curve stopped after two cycles with conventional constrained window. It is because that the printing process with the conventional constrained surface failed after two layers due to the excessive separation force. However, with the newly designed air-diffusion-channel-based constrained surface, it can be seen that the blue separation force curve

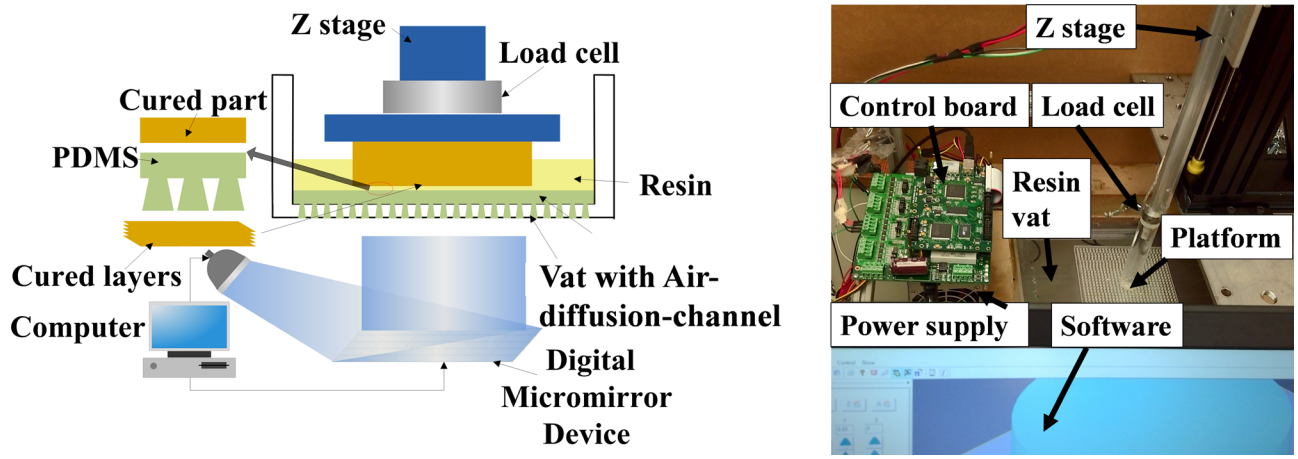

Fig. 9 Schematic of the bottom–up projection SL testbed (left) and a prototype setup (right)

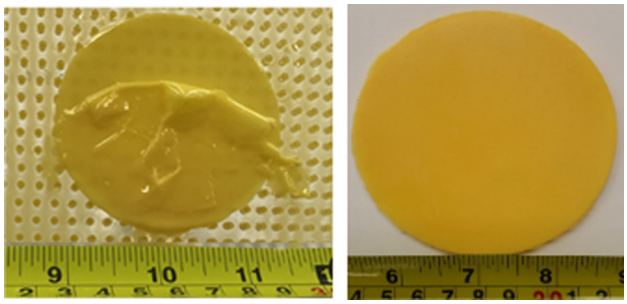

Fig. 11 Pictures of printed parts: (left) part failed at second layer using the conventional constrained surface; (right) part successfully printed with a thickness of 1.5 mm and a diameter of 90 mm using the newly developed air-diffusion-channel-based constrained surface

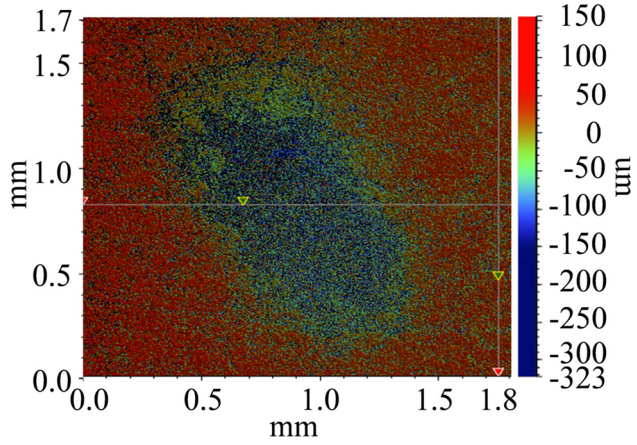

Fig. 12 Surface roughness measurement of a printed surface

dropped from the initial 100 N peak to 50 N peak in the second cycle and became stable in the following cycles. In addition, in the first cycle of the blue separation curve, its peak is half of the peak of the red curve. Pictures of the part which was failed at the second layer in the process using conventional constrained window and the part successfully printed by the newly designed constrained window are also shown in Fig. 11.

The measured separation forces and the solid object printing results shown in Figs. 10 and 11 verified that the micro-air channel design has a much higher and stable oxygen permeation and hence performs much better in production of solid objects with wide cross sections.

6.3 Surface Roughness of the Fabricated Samples. The surface quality of the printed parts was observed and characterized

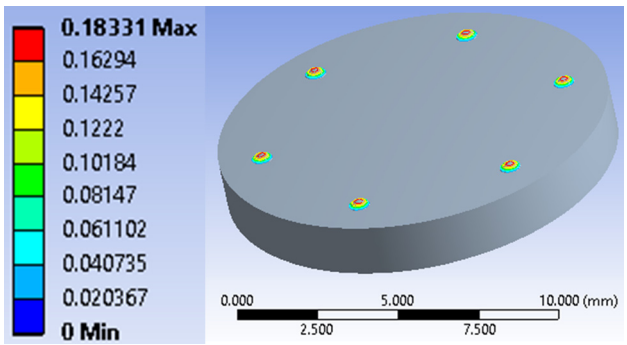

Fig. 13 Simulation of PDMS deformation when separation force is applied (vertical scale: −0.18 mm to 0 mm)

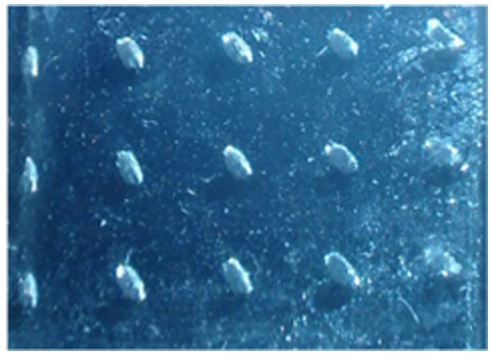

Fig. 14 Observed dots inside the projected image

using a 3D optical microscope from BRUKER (Billerica, MA). Regularly distributed dents were identified on the top surface of the part. A surface roughness measurement result of a dent region is shown in Fig. 12. It is found that the depth of the dents are ∼150 μm.

One possible cause of the dents on printed surface is that the PDMS near the air-diffusion-channel region deforms during the separation process, which then damages the related regions of the printed surface. To test this hypothesis, a simulation study was carried out using ANSYS WORKBENCH. In the simulation, a 13 mm diameter plate is modeled as PDMS. Fixed constraints are applied on the bottom surface of the PDMS plate except for the regions abut the air-diffusion-channel, and the side wall of the PDMS plate. A 7864 Pa pressure along the exterior normal of the PDMS top surface is applied. Simulation result is shown in Fig. 13. It shows that in order to obtain dents of ∼150 μm depth, at least a ∼178 N separation force is needed for each layer, and the diameter of the air-diffusion-channel should be bigger than 0.8 mm, which does not agree with the experimental settings, as the measured separation force for each layer was less than 80 N and the diameter of air-diffusion-channel used in the setup was only 0.25 mm.

Another possible cause of the dents is that the constrained surface is not perfectly perpendicular to the projected light, which causes the deflection of the light when passing through the air-diffusion-channel. For better observation, the constrained surface with air-diffusion-channel is tilted by ∼5 deg manually, and the light projection was observed. Little dots can be observed clearly around the air-diffusion-channel in the projection area, as shown in Fig. 14. Such shadowed image due to the alignment error of the constrained surface may cause the dents on the printed surfaces.

To address this dent printing problem, a careful leveling was done, to ensure that the constrained surface is well aligned with the projection focus plane. Then, a new part was printed using the same computer-aided design model, in the adjusted setup with the same process setting and the same newly designed constrained surface as used for the previous prints. A comparison of the two parts built before and after the constrained surface alignment adjustment is shown in Fig. 15. No more dents were observed in the newly printed part. Before adjustment, the measured roughness parameters are Ra = 56.167 μm and Rq = 68.83 μm, while a 0.49 μm Ra and a 0.673 μm Rq were observed after the adjustment. It indicated that leveling of the constrained surface is critical for ensuring the projection light uniformity and hence the printing quality.

7 Conclusions

This paper presented a constrained surface design with air-diffusion-channel, for constrained surface-based vat photopolymerization processes. Two different air-diffusion-channel designs have been investigated, and effects of the air-diffusion-channel design parameters on constrained surface properties and

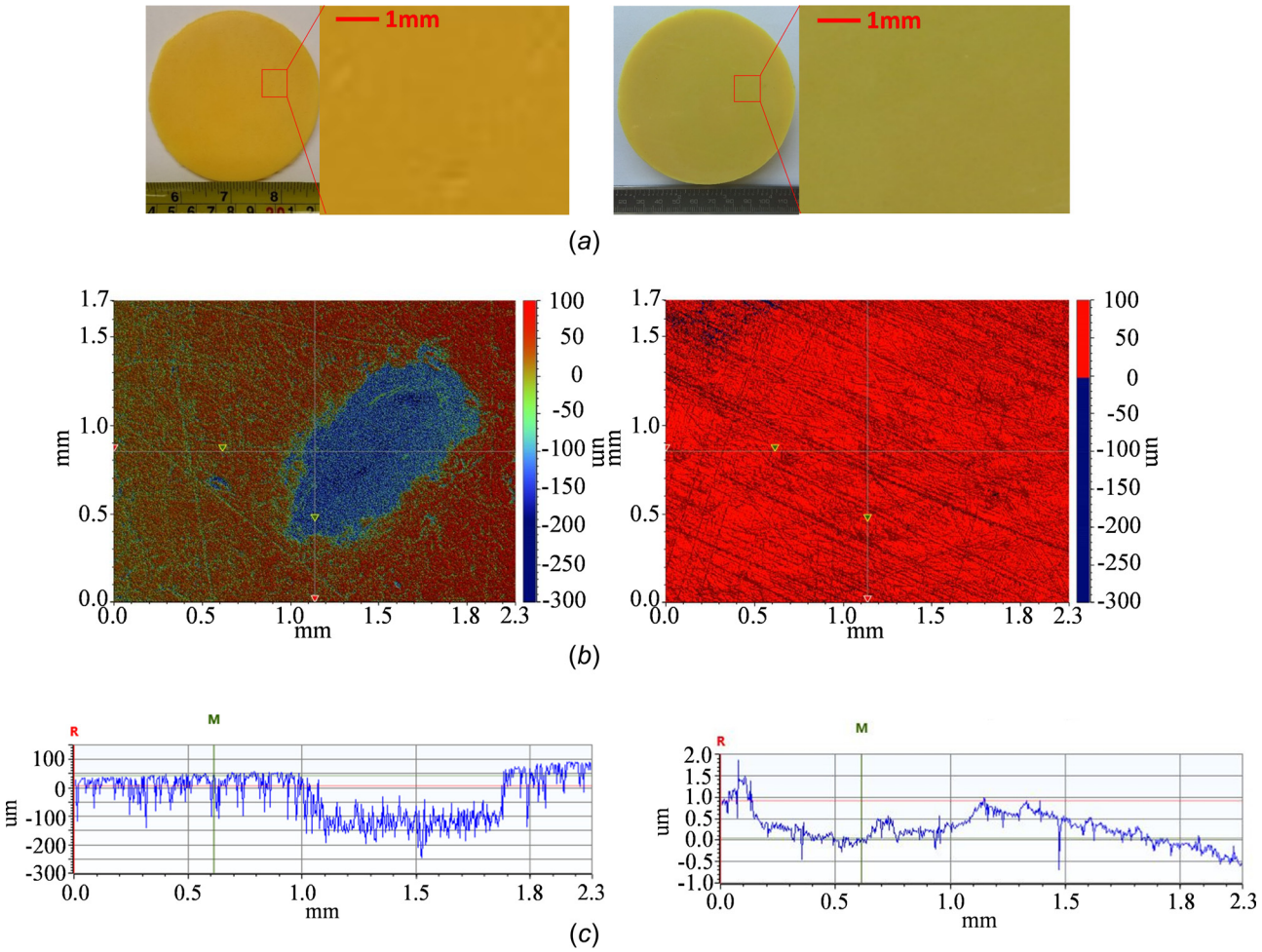

Fig. 15 Comparision between parts before and after adjustment

performances have been studied. It is found that the bonding strength between the PDMS coating and air-channel-incorporated substrate is stronger than that of the conventional PDMS-coated windows. Besides, very slight optical power decrease was observed in the proposed air-channel-based constrained surface. The principle of how the oxygen inhibition effect is enhanced by the proposed approach is analyzed and experimentally studied. It is found that the oxygen inhibition layer thickness increases approximately linearly with the air-channel area, and a 0.2 mm diameter air-channel design can form a $\sim$30 μm oxygen inhibition layer thickness, which is superior than the existing constrained surfaces. Experiments have been carried out to verify the effectiveness of the designed constrained surface in 3D printing. A solid cylinder with a 90 mm diameter is successfully built with our newly designed constrained surface. The effectiveness of the proposed method in printing wide solid cross section parts has been verified.

Acknowledgment

The authors would like to also acknowledge the Nanotechnology Core Facility of the University of Illinois at Chicago campus for training on and usage of the Bruker-Nano Model Contour GT-K Optical Profilometer.

Funding Data

- National Science Foundation (Grant No. 1563477).

References

[1] Grant, B., and Yao, Y. L., 2017, "Material Influence on Mitigation of Stress Corrosion Cracking Via Laser Shock Peening," ASME J. Manuf. Sci. Eng., **139**(1), p. 011002.
[2] Denlinger, E. R., Gouge, M., Irwin, J., and Michaleris, P., 2017, "Thermomechanical Model Development and In Situ Experimental Validation of the Laser Powder-Bed Fusion Process," Addit. Manuf., **16**, pp. 73–80.
[3] Gouge, M. F., Michaleris, P., and Palmer, T. A., 2016, "Fixturing Effects Thermal Modeling Laser Cladding," ASME J. Manuf. Sci. Eng., **139**(1), p. 011001.
[4] Wang, Q., Li, J., Gouge, M., Nassar, A. R., Michaleris, P. P., and Reutzel, E. W., 2016, "Physics-Based Multivariable Modeling and Feedback Linearization Control of Melt-Pool Geometry and Temperature in Directed Energy Deposition," ASME J. Manuf. Sci. Eng., **139**(2), p. 021013.
[5] Ye, H., Zhou, C., and Xu, W., 2017, "Image-Based Slicing and Tool Path Planning for Hybrid Stereolithography Additive Manufacturing," ASME J. Manuf. Sci. Eng., **139**(7), p. 071006.
[6] Song, X., Zhang, Z., Chen, Z., and Chen, Y., 2016, "Porous Structure Fabrication Using a Stereolithography-Based Sugar Foaming Method," ASME J. Manuf. Sci. Eng., **139**(3), p. 031015.
[7] Shusteff, M., Browar, A. E. M., Kelly, B. E., Henriksson, J., Weisgraber, T. H., Panas, R. M., Fang, N. X., and Spadaccini, C. M., 2017, "One-Step Volumetric Additive Manufacturing of Complex Polymer Structures," Sci. Adv., **3**(12), p. eaao5496.
[8] Song, X., Chen, Y., Lee, T. W., Wu, S., and Cheng, L., 2015, "Ceramic Fabrication Using Mask-Image-Projection-Based Stereolithography Integrated With Tape-Casting," J. Manuf. Process., **20**(Pt. 3), pp. 456–464.
[9] Yang, Y., Li, X., Zheng, X., Chen, Z., Zhou, Q., and Chen, Y., 2017, "3D-Printed Biomimetic Super-Hydrophobic Structure for Microdroplet Manipulation and Oil/Water Separation," Adv. Mater., **30**(9), p. 1704912.
[10] Nofal, M., Pan, Y., and Al-Hallaj, S., 2017, "Selective Laser Sintering of Phase Change Materials for Thermal Energy Storage Applications," Proc. Manuf., **10**, pp. 851–865.
[11] Chen, B., Jiang, Y., Tang, X., Pan, Y., and Hu, S., 2017, "Fully Packaged Carbon Nanotube Supercapacitors by Direct Ink Writing on Flexible Substrates," ACS Appl. Mater. Interfaces, **9**(34), pp. 28433–28440.
[12] Pan, Y., and Chen, Y., 2017, "Fast Mask Image Projection-Based Micro-Stereolithography Process for Complex Geometry," ASME J. Micro Nano-Manuf., **5**(1), p. 014501.
[13] Liravi, F., Das, S., and Zhou, C., 2015, "Separation Force Analysis and Prediction Based on Cohesive Element Model for Constrained-Surface Stereolithography Processes," Comput.-Aided Des., **69**, pp. 134–142.

[14] Pan, Y., Zhou, C., and Chen, Y., 2012, "A Fast Mask Projection Stereolithography Process for Fabricating Digital Models in Minutes," ASME J. Manuf. Sci. Eng., **134**(5), p. 051011.
[15] He, H., Pan, Y., Xu, J., Yu, X., and Botton, V., 2016, "Effect of Surface Texturing on Separation Force in Projection Stereolithography," 11th International Conference on Micro Manufacturing (ICOMM 2016), Irvine, CA, Mar. 29–31, p. 82.
[16] He, H., Pan, Y., Xu, J., and Yu, X., 2017, "Effect of Constrained Surface Texturing on Separation Force in Projection Stereolithography," Solid Freeform Fabrication Symposium (SFF), Austin, TX, Aug. 13–15, pp. 1735–1749.
[17] Lu, L., Guo, P., and Pan, Y., 2017, "Magnetic-Field-Assisted Projection Stereolithography for Three-Dimensional Printing of Smart Structures," ASME J. Manuf. Sci. Eng., **139**(7), p. 071008.
[18] Lu, L., Joyee, E. B., and Pan, Y., 2017, "Correlation Between Microscale Magnetic Particle Distribution and Magnetic-Field-Responsive Performance of Three-Dimensional Printed Composites," ASME J. Micro Nano-Manuf., **6**(1), p. 010904.
[19] Zhang, Y., Jariwala, A., and Rosen, D. W., 2015, "Effects of Oxygen Inhibition and Post-Processing on Exposure Controlled Projection Lithography Process Accuracy," Solid Freeform Fabrication Symposium, Austin, TX, pp. 346–359.
[20] Pan, Y., He, H., Xu, J., and Feinerman, A., 2017, "Study of Separation Force in Constrained Surface Projection Stereolithography," Rapid Prototyping J., **23**(2), pp. 353–361.
[21] Tumbleston, J. R., Shirvanyants, D., Ermoshkin, N., Janusziewicz, R., Johnson, A. R., Kelly, D., Chen, K., Pinschmidt, R., Rolland, J. P., Ermoshkin, A., and Samulski, E. T., 2015, "Continuous Liquid Interface Production of 3D Objects," Science, **347**(6228), pp. 1349–1352.
[22] Dendukuri, D., Panda, P., Haghgooie, R., Kim, J. M., Hatton, T. A., and Doyle, P. S., 2008, "Modeling of Oxygen-Inhibited Free Radical Photopolymerization in a PDMS Microfluidic Device," Macromolecules, **41**(22), pp. 8547–8556.
[23] Leclerc, E., Sakai, Y., and Fujii, T., 2004, "Microfluidic PDMS (Polydimethylsiloxane) Bioreactor for Large—Scale Culture of Hepatocytes," Biotechnol. Prog., **20**(3), pp. 750–755.
[24] Lamberti, A., Marasso, S. L., and Cocuzza, M., 2014, "PDMS Membranes With Tunable Gas Permeability for Microfluidic Applications," RSC Adv., **4**(106), pp. 61415–61419.
[25] Shiku, H., Saito, T., Wu, C. C., Yasukawa, T., Yokoo, M., Abe, H., Matsue, T., and Yamada, H., 2006, "Oxygen Permeability of Surface-Modified Poly (Dimethylsiloxane) Characterized by Scanning Electrochemical Microscopy," Chem. Lett., **35**(2), pp. 234–235.
[26] Tambe, N. S., and Bhushan, B., 2005, "Micro/Nanotribological Characterization of PDMS and PMMA Used for BioMEMS/NEMS Applications," Ultramicroscopy, **105**(1), pp. 238–247.
[27] Tan, H. Y., Loke, W. K., and Nguyen, N. T., 2010, "A Reliable Method for Bonding Polydimethylsiloxane (PDMS) to Polymethylmethacrylate (PMMA) and Its Application in Micropumps," Sens. Actuators B: Chem., **151**(1), pp. 133–139.
[28] Chow, W. W., Lei, K. F., Shi, G., Li, W. J., and Huang, Q., 2006, "Microfluidic Channel Fabrication by PDMS-Interface Bonding," Smart Mater. Struct., **15**(1), p. S112.
[29] Kawaguchi, M., Fukushima, T., and Miyazaki, K., 1994, "The Relationship Between Cure Depth and Transmission Coefficient of Visible-Light-Activated Resin Composites," J. Dent. Res., **73**(2), pp. 516–521.
[30] Grzybowski, B., Qin, D., Haag, R., and Whitesides, G. M., 2000, "Elastomeric Optical Elements With Deformable Surface Topographies: Applications to Force Measurements, Tunable Light Transmission and Light Focusing," Sens. Actuators A: Phys., **86**(1–2), pp. 81–85.
[31] Alobaidani, A. D., Furniss, D., Johnson, M. S., Endruweit, A., and Seddon, A. B., 2010, "Optical Transmission of PMMA Optical Fibres Exposed to High Intensity UVA and Visible Blue Light," Opt. Lasers Eng., **48**(5), pp. 575–582.
[32] Weng, Z., Zhou, Y., Lin, W., Senthil, T., and Wu, L., 2016, "Structure-Property Relationship of Nano Enhanced Stereolithography Resin for Desktop SLA 3D Printer," Compos. Part A: Appl. Sci. Manuf., **88**, pp. 234–242.
[33] Zguris, Z., 2018, "How Mechanical Properties of Stereolithography 3D Prints are Affected by UV Curing," Formlabs, Inc., Somerville, MA, accessed Nov. 4, 2017, https://formlabs.com/media/upload/How-Mechanical-Properties-of-SLA-3D-Prints-Are-Affected-by-UV-Curing.pdf
[34] Lee, M. P., Cooper, G. J., Hinkley, T., Gibson, G. M., Padgett, M. J., and Cronin, L., 2015, "Development of a 3D Printer Using Scanning Projection Stereolithography," Sci. Rep., **5**(1), p. 9875.
[35] Ashdown, I., 2016, "Sports Lighting Regulations," Lighting Analysts, Inc., Littleton, CO, accessed Dec. 24, 2017, http://agi32.com/blog/tag/uniformity-ratio/
[36] Lee, H. W., and Lin, B. S., 2012, "Improvement of Illumination Uniformity for LED Flat Panel Light by Using Micro-Secondary Lens Array," Opt. Express, **20**(106), pp. A788–A798.
[37] Singh, A., Freeman, B. D., and Pinnau, I., 1998, "Pure and Mixed Gas Acetone/Nitrogen Permeation Properties of Polydimethylsiloxane [PDMS]," J. Polym. Sci. Part B: Polym. Phys., **36**(2), pp. 289–301.
[38] Thomas, P. C., Raghavan, S. R., and Forry, S. P., 2011, "Regulating Oxygen Levels in a Microfluidic Device," Anal. Chem., **83**(22), pp. 8821–8824.
[39] Rao, H. X., Liu, F. N., and Zhang, Z. Y., 2007, "Preparation and Oxygen/Nitrogen Permeability of PDMS Crosslinked Membrane and PDMS/Tetraethoxysilicone Hybrid Membrane," J. Membr. Sci., **303**(1–2), pp. 132–139.
[40] Merkel, T. C., Bondar, V. I., Nagai, K., Freeman, B. D., and Pinnau, I., 2000, "Gas Sorption, Diffusion, and Permeation in Poly (Dimethylsiloxane)," J. Polym. Sci. Part B: Polym. Phys., **38**(3), pp. 415–434.